HHS Public Access

Author manuscript

Environ Sci Technol. Author manuscript; available in PMC 2016 March 07.

Published in final edited form as:

Environ Sci Technol. 2015 July 7; 49(13): 8048–8056. doi:10.1021/acs.est.5b01214.

Static and dynamic microscopy of the chemical stability and aggregation state of silver nanowires in components of *murine* pulmonary surfactant

Ioannis G. Theodorou[a], **Danielle Botelho**[b], **Stephan Schwander**[c], **Junfeng (Jim) Zhang**[d], **Kian Fan Chung**[e], **Teresa D. Tetley**[e], **Milo S. P. Shaffer**[f], **Andrew Gow**[b], **Mary P. Ryan**[*,a], and **Alexandra E. Porter**[**,a]

[a]Department of Materials and London Centre for Nanotechnology, Imperial College London, Exhibition Road, London SW7 2AZ, United Kingdom

[b]Department of Pharmacology and Toxicology, Rutgers University, Piscataway, New Jersey 08854, United States

[c]Rutgers School of Public Health, Department of Environmental and Occupational Health, Piscataway, New Jersey 08854, United States

[d]Nicholas School of the Environment and Duke Global Health Institute, Duke University, Durham, NC 27708, United States

[e]National Heart and Lung Institute, Imperial College London, London SW3 6LY, United Kingdom

[f]Department of Chemistry and London Centre for Nanotechnology, Imperial College London, Exhibition Road, London SW7 2AZ, United Kingdom

Abstract

The increase of production volumes of silver nanowires (AgNWs) and of consumer products incorporating them, may lead to increased health risks from occupational and public exposures. There is currently limited information about the putative toxicity of AgNWs upon inhalation, and incomplete understanding of the properties that control their bioreactivity. The lung lining fluid (LLF), which contains phospholipids and surfactant proteins, represents a first contact site with the respiratory system. In this work, the impact of Dipalmitoylphosphatidylcholine (DPPC), Curosurf® and *murine* LLF on the stability of AgNWs was examined. Both the phospholipid and protein components of the LLF modified the dissolution kinetics of AgNWs, due to the formation of a lipid corona or aggregation of the AgNWs. Moreover, the hydrophilic, but neither the hydrophobic surfactant proteins nor the phospholipids, induced agglomeration of the AgNWs. Finally, the generation of a secondary population of nano-silver was observed and attributed to the reduction of Ag^+ ions by the surface capping of the AgNWs. Our findings highlight that combinations of spatially resolved dynamic and static techniques are required to develop a holistic

[*]m.p.ryan@imperial.ac.uk. [**]a.porter@imperial.ac.uk.

Supporting Information

Experimental protocols. This material is available free of charge via the Internet: http://pubs.acs.org.

understanding of which parameters govern AgNW behavior at *the point of exposure* and to accurately predict their risks on human health and the environment.

Keywords

silver nanowires; lung surfactant; corona; phospholipids; surfactant proteins

Introduction

One-dimensional nanomaterials are attracting increasing attention due to their unique physicochemical properties.[1] Silver nanowires (AgNWs) are considered as the potential building blocks for the next generation of optical, electronic and sensing devices.[2] The increase in production and use of AgNWs has led to growing concerns about the potential adverse effects on human health upon exposure to AgNWs. Although occupational exposures to AgNWs during production, packaging or processing may be higher, general public exposures are also possible, given the increasing use of AgNW-containing consumer products (*e.g.* spray coatings, personal electronics). One of the primary routes for exposure is inhalation of airborne AgNWs. Upon inhalation, spherical nanoparticles (NPs) with diameters between 10 and 100 nm have maximum deposition in the alveolar region of the lung.[3] For fibrous nanomaterials (NMs), like AgNWs, their width is the key parameter that affects their lung deposition pattern, due to the central role of fiber diameter in controlling the aerodynamic diameter (D_{ae}) and the dependence of pulmonary deposition on D_{ae}.[4] According to one model, fibers with diameters < 100 nm, independent of their length, preferentially deposit in intermediately to terminally situated lung airways, with a peak alveolar deposition between 10% and 20%. In the alveoli, where removal is dominated by slow, macrophage-mediated clearance,[5] fibers have the potential to contribute most to builtup of dose.

Consequently, fibrous NMs, including AgNWs, have raised concerns due to the comparisons with asbestos fibers in the lung and the induced mesothelioma.[6, 7] *In vitro* work revealed that AgNWs were more toxic than spherical AgNPs on alveolar epithelial cells.[8] Recently, AgNWs were shown to produce dose-dependent inflammation in *murine* lungs and responses dependent on both AgNW length and dissolution rates.[9] The toxicity of AgNWs has not been thoroughly investigated and discrepancies still exist on the mechanism of biological action of AgNMs in general.[10, 11] The lack of consistency could be in part due to the fact that most studies have not considered the fate of AgNMs in biologically relevant environments and alterations to the physicochemical properties of as-synthesized NMs. This has been highlighted in our recent work that revealed the sulfidation of AgNWs in cell culture media[12] as well as inside human alveolar epithelial type 1-like cells.[13] Due to the extremely low solubility of Ag_2S, the Ag^+ ion release rate will be substantially reduced; therefore reduced AgNW toxicity could be expected. Hence, in order to draw accurate conclusions about the bioreactivity of AgNWs, it is vital to characterize their physicochemical properties at the *point of exposure*. For AgNWs that reach the alveolar region of the lung, this first point of contact will be the lung lining fluid (LLF).

The LLF is a thin liquid layer (<0.1-0.2 μm) that covers and protects the epithelial cells in the alveoli. Its main component is surfactant, which forms a monolayer at the liquid-air interface. The most abundant component of surfactant (70-80% of total lipids) is phosphatidylcholine (PC), about 50% of which is saturated, especially in the dipalmitoylated form (DPPC).[14] Furthermore, four surfactant-associated proteins have been described: the hydrophilic SP-A and SP-D and the hydrophobic SP-B and SP-C.[15] Inhaled AgNWs that enter and deposit in the alveoli may adsorb LLF components, affecting their subsequent cellular effects.[16, 17] Studies indicate that the LLF layer may promote interaction of inhaled particles with the underlying epithelium, through wetting forces that draw the particles into the surfactant toward the alveolar wall.[18, 19] The effects of the LLF on the physicochemistry of AgNWs will determine their interaction with proteins, cells and tissues in the lung. An altered aggregation state could modify particle transport, the amount of AgNWs internalized by cells and subsequent interactions within cells.[20] Moreover, AgNWs could alter the surface tension of the lung surfactant and affect immune responses by sequestering lipids or proteins.[21] In our group, we have demonstrated that AgNPs incubated with DPPC were coated by a phospholipid corona, which delayed oxidative dissolution of AgNPs and inhibited aggregation and coarsening.[22] However, few data exist on the stability of AgNMs in other components of the LLF or in LLF from an animal model.

The purpose of this study is to characterize the impact of individual components of the LLF on the stability of AgNWs (grown *in-house* to ensure a full control of their initial physicochemistry). Phospholipids, as well as each class of surfactant-associated proteins, the hydrophobic SP-B/C and the hydrophilic SP-A/D, were separately added to AgNWs in an effort to delineate their effects on the properties of AgNWs. These effects were investigated at different pH values, representative of environments found in the lung and that mimic endocytotic conditions.

Inductively Coupled Plasma–Optical Emission Spectroscopy (ICP-OES), *in situ* optical microscopy and a combination of analytical transmission electron microscopy (TEM) techniques were used to investigate the dissolution, colloidal stability and surface chemistry of AgNWs. The use of correlative imaging techniques, which provide both dynamic and spatially resolved information about the chemistry of the AgNWs, enabled us to directly visualize the impact of the LLF components on the surface chemistry of AgNWs, agglomeration states as well as the structure of the lipid corona. The advantages of using TEM are its ability to provide spatially resolved information about the distribution of crystal phases, the structure of the lipid corona and the crystallinity of small nanomaterials.

Materials and Methods

AgNWs were synthesized in-house by a modified polyol process.[23]

AgNW incubations in LLF components

1,2-dipalmitoyl-sn-glycero-3-phosphocholine (DPPC) was purchased from Sigma-Aldrich. Curosurf®, a natural surfactant containing phospholipids and SP-B/C, was donated by Chiesi Farmaceutici. *Murine* LLF was extracted by bronchoalveolar lavage and fractionated to the large aggregate (LA) portion, which contains phospholipids and SP-B/C, and the small

aggregate (SA) portion, which contains soluble lung proteins, including SP-A/D. AgNWs (25 μg/mL) were incubated in various combinations of these components. Complete LLF was obtained by recombining the LA and SA fractions. DPPC was used to study the effect of phospholipids, while Curosurf® and SA were used to investigate the effects of the hydrophobic (SP-B/C) and hydrophilic (SP-A/D) surfactant-associated proteins, respectively. AgNWs were incubated at pH 7 and pH 5 in sodium perchlorate ($NaClO_4$•H_20, Sigma-Aldrich) buffers, at 37 °C, for 1 hour up to 336 hours, in a dri-block incubator in the dark.

Scanning Electron Microscopy (SEM) was performed on a LEO 1525 Field Emission Gun SEM (FEG-SEM, Carl Zeiss Microscopy GmbH, UK), to study the morphology and size distribution of as-synthesized AgNWs.

Transmission Electron Microscopy (TEM)—The morphology and chemistry of as-synthesized AgNWs and AgNWs incubated with components of the LLF were examined by various analytical TEM techniques. Following washing of AgNWs with deionized water to remove excess salts or organic molecules, TEM samples were prepared on holey carbon film TEM grids, and stored under vacuum in the dark. Bright field TEM (BFTEM), high resolution TEM (HRTEM) and high angle annular dark field scanning transmission electron microscopy (HAADF-STEM), combined with selected area electron diffraction (SAED) and energy-dispersive X-ray spectroscopy (EDX) were performed on a JEOL JEM-2100F fitted with an EDX detector (Oxford Instruments).

Light Microscopy (LM) was employed to examine the aggregation states of AgNWs. Aliquots of AgNWs were placed on clean glass slides; coverslips were applied and the samples were imaged immediately with a Leica DM2500 light microscope.

Inductively Coupled Plasma–Optical Emission Spectroscopy (ICP-OES, Thermo Scientific, UK) with a silver detection limit of 0.6 μg/L was used to measure free Ag^+ ion concentrations.

Full details of the experimental protocols are provided in the SI.

Results

Characterization of as-synthesized AgNWs

It is vital to characterize the chemistry and crystalline structure of AgNWs in ambient conditions, as our previous work has shown that the chemistry of AgNWs changes if they are exposed to the environment.[13] Scanning electron microscopy (SEM) of the as-synthesized product showed that it is composed only of nanowires (Figure 1a). The length distribution of AgNWs, measured from several representative SEM images using ImageJ software, had an average of 1.5 ± 1.4 μm (Figure 1b), while the diameter distribution had an average of 79 ± 21 nm (Figure 1c). Bright Field Transmission Electron Microscopy (BFTEM) (Figure 1d) revealed a pentagonal cross-section of the wires, since AgNWs synthesized by the polyol process grow from five-fold twinned Ag seeds formed at the early stages of the reaction.[24] The lattice fringe spacings measured from phase contrast High

Resolution TEM (HRTEM) images (Figure 1e), were 2.36 ± 0.04 and 2.10 ± 0.04 Å, which correspond to the interplanar spacing of bulk Ag (111) and (200) lattice planes, respectively (ref. # 01-087-0597). The interplanar spacings measured from SAED patterns (Figure 1f) were 2.35 ± 0.04, 2.04 ± 0.02, 1.43 ± 0.01 and 1.22 ± 0.01 Å, which are consistent with the bcc form of bulk Ag (ref. # 01-087-0597). The presence of an amorphous layer of 1.2 ± 0.3 nm on the surface of AgNWs (Figure 1e) corresponds to the PVP coating (Figure 1d). Finally, STEM/EDX shows that the NWs are composed of pure Ag (Figure 1g, h) and confirms the absence of impurities in the synthesized product.

Ag^+ ion release kinetics in LLF—One of the main mechanisms of AgNM toxicity is postulated to be their dissolution and release of free Ag^+ ions.[25, 26] In order to understand discrepancies in previous studies, it is important to characterize the effect of relevant media on Ag^+ ion release kinetics. AgNW dissolution in the absence of LLF components was strongly pH-dependent (Figure 2a). At pH7, Ag^+ release was negligible, and appeared to decrease over time, which could be correlated with the formation of AgNPs as discussed in the section "*Generation of secondary AgNPs*". On the other hand, pH 5 resulted in a higher ion release rate, as has been reported for citrate-AgNPs.[22] In the presence of complete LLF at pH7, no significant differences in the amounts of Ag^+ ions released were measured. In accordance to this finding, individual components of the LLF (DPPC ± SA, Figure 2b and Curosurf ± SA, Figure 2c) had no effect on the amount or rate of Ag^+ ions released at pH7. At pH 5, however, the presence of LLF led to a lower AgNW dissolution, with the amounts of Ag^+ ions measured from 24 hours onward being about half compared to the absence of LLF (Figure 2a). This decrease in dissolution was further investigated by incubating AgNWs in combinations of individual LLF components (Figure 2b, c). Both DPPC and Curosurf® imparted a retarding effect to AgNW dissolution, with the amount of Ag^+ released after 24 hours being about half compared with AgNWs in pH 5 buffer. A similar effect has previously been described for citrate-capped AgNPs with DPPC.[22] With DPPC, this retarding effect lasted for 1 week, when there was little difference in the amount of Ag dissolved compared to AgNWs without DPPC. The effect was more pronounced with Curosurf®: it took two weeks for the amount of Ag^+ ions to reach the same concentration as with AgNWs in pH 5 buffer. Finally, addition of the SA, to both DPPC and Curosurf®, at pH5, resulted in a further decrease of the dissolved Ag^+ measured after 1 and 2 weeks. Under all conditions, the maximum concentration of free Ag^+ ions measured was 0.625 μg/mL, which is very low and unlikely to be toxic to cells. Acording to Cronholm *et al.*, 1 μg/mL of Ag^+ (added as $AgNO_3$) did not cause a significant increase in cell death in human lung cell lines (A549 and BEAS-2B).[27]

Morphology and aggregation states in LLF

The aggregation states of AgNWs as a function of pH, incubation time and LLF components were investigated using optical microscopy while their morphological evolution was studied by TEM. Optical microscopy allowed to preserve the native aqueous environment of AgNWs and avoid drying-induced artifacts during sample preparation for electron microscopy. Incubation of AgNWs in complete LLF (Figure 3a), at both pH7 (Figure 3a, i-iii) and pH5 (Figure 3a, iv-vi) led to agglomeration of the wires, which was evident after 24 hours (Figure 3a, ii and v) and 7 days (Figure 3a, iii and vi). AgNWs were then incubated in

individual LLF components, to examine which are responsible for the observed agglomeration. In the absence of biomolecules, incubation at both pH 7 (Figure 3b, i and ii) and pH 5 (Figure 3b, vi and vii) for 1 hour (Figure 3b, i and vi) up to 1 week (Figure 3b, ii and vii), led to no observable differences in the aggregation state of AgNWs; AgNWs appeared as single wires randomly dispersed in solution. The addition of DPPC (Figure 3b, iii and viii), Curosurf® (Figure 3b, iv and ix) or the LA (Figure 3b, v and x) had no effect on the apparent dispersion of AgNWs. These observations are in agreement with our previous work, where small angle X-ray scattering (SAXS) data indicated that DPPC prevented AgNPs from agglomeration.[22] However, addition of the SA to Curosurf®, at both pH 7 (Figure 3c, i-iii) and pH 5 (Figure 3c, iv-vi), resulted to agglomeration of the wires, observed from 24 hours of incubation (Figure 3c, ii and v). To compare with previous findings, where incubation of citrate-AgNPs at pH 5 resulted to aggregation and coarsening of the NPs,[22] TEM imaging was performed, but no pH-induced coarsening of the AgNWs was observed (Figure 3d). In contrast to citrate-capped AgNPs, AgNWs remain dispersed due to the steric stabilization by the PVP polymer capping, instead of the electrostatic stabilization provided by citrate ions.[28] Analysis by STEM/EDX provided no evidence for changes in the crystal structure of the AgNWs in any of the LLF components. Most importantly, sulfur sources have previously been implicated in the formation of Ag_2S on the surface of AgNWs.[12, 29] Incubation of AgNWs with SA, which includes the thiol-containing SP-A and SP-D proteins, did *not* result in precipitation of Ag_2S (Figure 3d, e, ≥100 AgNWs analyzed). This is in agreement with previous findings where, although AgNWs were readily sulfidized by inorganic sulfur species, they were *not* by sulfur containing amino acids or proteins, such as cysteine or bovine serum albumin.[12]

Characterization of phospholipid corona

TEM imaging provided further insights into the effects of phospholipids on the stability of AgNWs. Incubation with DPPC increased the thickness of the amorphous layer present around the AgNWs (Figure 4b) to an average of 7.6 ± 5.2 nm, compared to that of AgNWs in the absence of phospholipid components (Figure 4a), which was attributed to the coating of AgNWs by phospholipids. Their organization on the surface of AgNWs was revealed using uranyl acetate positive staining, which takes advantage of the high affinity of electron dense uranyl ions for the phosphate groups in phospholipids[30], enhancing contrast. AgNWs incubated with DPPC, Curosurf® or the LA showed striations that are parallel to the long axis of the AgNWs (Figure 4c, d, f, g). The hydrophilic headgroup of the DPPC molecule is expected to produce dark contrast whereas the two hydrophobic fatty acid tails will show bright contrast.[30] Therefore, a lipid bilayer structure was formed on the surface of AgNWs, with the hydrophobic tails of DPPC associated with each other and the hydrophilic head-groups oriented toward the aqueous environment and the PVP layer, which is also hydrophilic. The average bilayer thickness, measured from several intensity line profiles (Figure 4e), was 3.8 ± 0.5 nm, which is close to the hydrocarbon bilayer thickness of 4.16 nm calculated by Park et al.[31] The hydrophobic fatty acid tails of the DPPC molecule are comprised by 16 hydrocarbons. Assuming that the carbon chains are stretched and a chain length between one carbon and the next of 1.3 Å, they estimated the maximum length of DPPC at 2.08 nm and thus 4.16 nm for a bilayer.[31] The average DPPC bilayer thickness previously measured by AFM was 5.0 nm, and was shown to vary as a function of

temperature and analysis technique.[32] The DPPC bilayer thickness on citrate-AgNPs measured by TEM was 4.3 nm.[22] STEM/EDX analysis at the surface of AgNWs (Figure 4h) revealed the presence of phosphorous (Figure 4i), while STEM/EDX elemental mapping for silver (Figure 4j) and phosphorous (Figure 4k) confirmed that AgNWs were coated by phospholipids (Figure 4l).

Generation of secondary AgNPs

The generation of a secondary population of NPs in all of the test solutions was also observed by TEM. After 24 hours, small particles appeared close to the PVP coating of AgNWs (Figure 5a, b), whereas in the presence of DPPC, inside the phospholipid layer (Figure 5d-e). After 7 days, a larger amount of NPs was observed (Figure 5c, d, 6a). Analysis of their chemistry by STEM/EDX revealed only the presence of Ag (Figure 6b) (the silicon (Si) peak is due to Si contamination of the carbon grids)[33]. Since the buffers used for the incubation of the AgNWs only contained perchlorate ions, precipitation of insoluble Ag compounds such as Ag_2O, AgCl, Ag_2S or Ag_3PO_4 could not have occurred in solution. STEM/EDX elemental mapping (Figure 6c) excluded the formation of these Ag compounds as a result of environmental contaminations during the experiments. HRTEM (Figure 6d) revealed a lattice spacing of 2.37 ± 0.07 Å, which corresponds to the interplanar spacing of bulk Ag (111) (ref. # 01-087-0597), confirming that the particles are metallic AgNPs. More than 100 particles were analyzed in each sample, and all were shown to be Ag NPs.

These AgNPs were never detected in as-synthesized samples, by neither SEM (Figure 1a) nor TEM/STEM (Figures 1d, e, g). When AgNWs were incubated in perchlorate buffers where dissolved oxygen had been removed by purging with argon to inhibit oxidative dissolution of AgNWs,[34] no NPs could be observed after 2 weeks, suggesting that the AgNPs are formed from a reprecipitation of dissolved Ag^+ ions. Since all the experiments were performed in the dark and no other reducing agent was present in solution, the reduction of Ag^+ ions to form AgNPs was attributed to the mild reducing capabilities of the PVP stabilizer.[35, 36] Previous studies also reported that Ag^+ ions released from AgNPs were reduced by PVP and formed a secondary population of smaller AgNPs.[37, 38] Their size evolution (more than 300 particles measured in each case) as a function of time shows a slight increase after 2 weeks of incubation at pH 7 compared to 24 hours (Figure 6e). AgNPs formed at early incubation times probably serve as seeds that grow in size as more Ag^+ ions are released from AgNWs. AgNPs formed after 24 hours at pH 5 had a slightly larger size compared to pH 7, (Figure 6f), possibly due to the higher rate of Ag^+ ion release from AgNWs at pH 5. After 2 weeks, their size decreased, possibly due to dissolution of AgNPs themselves, which is faster at pH 5.

Discussion

The propensity for the physicochemical properties of AgNMs to alter, in some cases quite radically, depending on the environment they encounter, can significantly alter their bioreactivity with the environment, cells and tissues. Therefore, in order to understand the mechanisms of biological action of Ag nanomaterials, these transformations must be

thoroughly examined. In the present work, by performing careful characterization using both *in situ* techniques to track dynamic information about the colloidal stability of the AgNWs and spatially resolved high resolution elemental analysis, we were able to deconvolute the system parameters (*i.e.* pH, phospholipids, surfactant proteins, and capping agents) and provide new insights, on the effects of each parameter on the stability of AgNWs.

In summary, we have shown for the first time, *ex vivo* adsorption of surfactant lipids on AgNWs. This lipid corona delayed the kinetics of Ag^+ ion release from AgNWs. TEM imaging indicated that the adsorbed phospholipids form a coating on the surface of AgNWs and that the hydrophobic alkyl chains of the phospholipids are adsorbed onto the AgNWs while with the polar headgroups face away from the AgNWs toward the aqueous phase. Moreover, using *in situ* light microscopy, we have demonstrated that the small aggregate fraction of the LLF was responsible for the agglomeration of the AgNWs observed in LLF and the decreased release of Ag^+ ions. We have also shown the generation of a secondary population of AgNPs from the original AgNWs, possibly due to the reduction of Ag^+ ions by the PVP capping of the wires.

Effect of pH

The release of free Ag^+ ions is often considered as the predominant mechanism of toxicity for AgNMs. In the endocytic pathway, the pH progressively decreases from about 7.1 to lower than 5.5 in lysosomes, which could affect the extent of Ag dissolution in different cellular compartments. The dissolution of AgNPs is considered to be *via* a cooperative oxidation that involves both protons and dissolved oxygen:[34]

$$2Ag_{(s)}+\frac{1}{2}O_{2(aq)}+2H^+{}_{(aq)} \iff 2Ag^+{}_{(aq)}+H_2O_{(l)}$$

In our experiments, dissolution of AgNWs was carried out under ambient atmosphere and therefore dissolved oxygen is a possible factor in the oxidation of AgNWs. It is also clear from our data that the *kinetics* of AgNW dissolution *are* affected by the pH. Similar observations have been made for both citrate[22, 34] and PVP capped AgNPs.[38] However, the maximum concentrations of Ag^+ ions measured, are not likely to significantly contribute to the toxicity of AgNWs.[27]

Effect of phospholipids

The presence of phospholipids, in either simple (DPPC) or complex mixtures (Curosurf®), induced a retarding effect on the release of Ag^+ ions at pH 5, which could be explained by the formation of phospholipid layers on the surface of AgNWs. This finding supports our previous work, where DPPC coating of citrate-AgNPs delayed Ag^+ ion release and prevented aggregating and coarsening.[22] We suggested that the DPPC coating acts as a diffusion barrier to molecular oxygen, decreasing the ion release kinetics. Here, we suggest that the outermost surface of the lipid coating corresponds to the hydrophilic headgroup of DPPC. When strongly hydrophilic groups interact with the surrounding aqueous media, the sorption of the organic compounds facilitates the stability of the nano-Ag dispersion.[39] This observation can now explain previous findings where the bronchoalveolar lavage improved

the dispersion of AgNPs.[40] The adsorption of lipids on AgNWs could directly affect their uptake by cells and the intracellular responses, which is the subject of ongoing research in our group. Research on other classes of nanomaterials has shown, for instance, that lipid adsorption led to increased internalization of TiO_2 NPs[41] and SWCNTs[42] by macrophages. In a recent study, human LLF increased the uptake of polystyrene NPs by human alveolar epithelial cells, regardless of NP size or surface modification.[43] Moreover, coating MWCNTs[44] or SWCNTs[45] with lipids evoked an increase in intracellular reactive oxygen species (ROS) production.

Effect of surfactant-associated proteins

The addition of SA further reduced the amount of Ag^+ ions released, which explains the decreased dissolution observed at pH5 in the presence of complete LLF. This decrease in dissolution was not due to a chemical transformation of the AgNWs, since sulfidation by the thiol containing SP-A and SP-D was ruled out by HRTEM and STEM/EDX. However, SA induced agglomeration of the AgNWs, at both pH values tested, consequently lowering the available surface area and thus the dissolution rate. Recent work has similarly demonstrated that incubation of various types of NPs with SP-A/D led to NP agglomeration,[46, 47] possibly through the selective binding of SP-A and/or SP-D to the NPs.[43, 48, 49] In our unpublished work, Western blot analysis showed that SP-A/D specifically binds to AgNWs. Protein adsorption on AgNWs could have implications on the bioreactivity of AgNWs upon inhalation, since for other types of NPs this altered their cellular uptake, clearance, translocation and toxic effects.[49] Changes in the agglomeration state of AgNWs may lead to different responses by different cell types. For example, lung epithelial (C-10) cells were found to be more resistant to AgNPs than macrophages (RAW-264.7).[50] This was attributed to the fact that the aggregate size of AgNPs in the cell culture medium was more than 100 nm, which improved their uptake efficiency by macrophages but reduced it by epithelial cells.[51] In the recent work by Silva *et al.*, instillation of AgNWs in rats led to the deposition of AgNWs in the deep lungs.[9] Both AgNW lengths tested produced significant numbers of Ag-positive macrophages at Day 1.[9] Herein, sp-A/D induced agglomeration of the AgNW also within 24 hours, which could therefore be responsible for the high uptake of AgNWs by macrophages in the Silva study.

Effect of capping agent

The generation of a secondary population of AgNPs from the original AgNWs was observed following their incubation at pH 7 and pH 5 and in the presence of LLF components. PVP-capped AgNPs have also been shown to generate smaller AgNPs when exposed to high relative humidities[37] or in solution.[38] Surface coatings may have a vast influence on the toxicological potential of AgNMs, as has been recently highlighted in a study where citrate-AgNPs were more toxic than PVP-AgNPs, despite having similar sizes and dissolution rates.[52] The authors proposed that Ag^+ ions form complexes with PVP, which reduces their bioavailability and consequently cytotoxicity. In the present work we show that Ag^+ ions may also undergo PVP-mediated reduction to form secondary AgNPs. These secondary particles, having a much smaller size, could directly interfere with the function of cell membranes, allowing a larger number of AgNPs to penetrate inside cells.[52] Smaller AgNPs may also be able to reach internal organelles more easily, inducing more pronounced toxic

effects.[53] Due to their smaller size, they are also expected to have enhanced dissolution kinetics.[54]

In conclusion, our findings show that different components of the LLF can significantly alter the aggregation state and surface chemistry of AgNWs. This is important as these alterations may change their reactivity and how they are internalized and processed by the underlying epithelial cells or macrophages. We are currently investigating this hypothesis. More generally, these observations highlight the need for detailed dynamic and static characterization at the point of exposure in order to develop a holistic understanding into which parameters govern AgNW bioreactivity, as the *in situ* properties of AgNWs may prevail over their inherent properties. Improving our understanding on how the physicochemical properties of AgNMs change in the presence of biomolecules is paramount for appreciating their true environmental and human health impact.

Supplementary Material

Refer to Web version on PubMed Central for supplementary material.

Acknowledgements

This work was funded in part by a grant from the NIEHS (grant number U19ES019536) and the US EPA/NERC (EPA STAR RD83469301 and NERC) and an ERC starting grant to AP (project number 257182).

References

1. Xia Y, Yang P, Sun Y, Wu Y, Mayers B, Gates B, Yin Y, Kim F, Yan H. One-Dimensional Nanostructures: Synthesis, Characterization, and Applications. Advanced Materials. 2003; 15:353–389.
2. Melosh NA, Boukai A, Diana F, Gerardot B, Badolato A, Petroff PM, Heath JR. Ultrahigh-density nanowire lattices and circuits. Science. 2003; 300:112–5. [PubMed: 12637672]
3. Human respiratory tract model for radiological protection. A report of a Task Group of the International Commission on Radiological Protection. Annals of the ICRP. 1994; 24:1–482.
4. Kreyling, WG.; Moller, W.; Semmler-Behnke, M.; Oberdorster, G. Particle dosimetry: Deposition and clearance from the respiratory tract and translocaton to extra-pulmonary sites. In: Donaldson, K.; Borm, P., editors. Particle Toxicology. CRC Press; Boca Raton, FL: 2007. p. 47-74.
5. Schlesinger, RB.; Ben-Jebria, A.; Dahl, AR.; Snipes, MB.; Ultman, J. Disposition of inhaled toxicants. In: Massaro, EJ., editor. Handbook of Human Toxicology. CRC Press; Boca Raton, FL: 1997. p. 493-550.
6. Donaldson K, Murphy F, Schinwald A, Duffin R, Poland CA. Identifying the pulmonary hazard of high aspect ratio nanoparticles to enable their safety-by-design. Nanomedicine : nanotechnology, biology, and medicine. 2010; 6:143–156.
7. Schinwald A, Donaldson K. Use of back-scatter electron signals to visualise cell/nanowires interactions in vitro and in vivo; frustrated phagocytosis of long fibres in macrophages and compartmentalisation in mesothelial cells in vivo. Particle and fibre toxicology. 2012; 9:34. [PubMed: 22929371]
8. Stoehr LC, Gonzalez E, Stampfl A, Casals E, Duschl A, Puntes V, Oostingh GJ. Shape matters: effects of silver nanospheres and wires on human alveolar epithelial cells. Particle and fibre toxicology. 2011; 8:36. [PubMed: 22208550]
9. Silva RM, Xu J, Saiki C, Anderson DS, Franzi LM, Vulpe CD, Gilbert B, Van Winkle LS, Pinkerton KE. Short versus long silver nanowires: a comparison of in vivo pulmonary effects post instillation. Particle and fibre toxicology. 2014; 11:52. [PubMed: 25292367]

10. Xiu ZM, Zhang QB, Puppala HL, Colvin VL, Alvarez PJJ. Negligible Particle-Specific Antibacterial Activity of Silver Nanoparticles. Nano Lett. 2012; 12:4271–4275. [PubMed: 22765771]
11. Yin L, Cheng Y, Espinasse B, Colman BP, Auffan M, Wiesner M, Rose J, Liu J, Bernhardt ES. More than the ions: the effects of silver nanoparticles on Lolium multiflorum. Environmental science & technology. 2011; 45:2360–7. [PubMed: 21341685]
12. Chen S, Theodorou IG, Goode AE, Gow A, Schwander S, Zhang J, Chung KF, Tetley TD, Shaffer MS, Ryan MP, Porter AE. High-Resolution Analytical Electron Microscopy Reveals Cell Culture Media-Induced Changes to the Chemistry of Silver Nanowires. Environmental science & technology. 2013; 47:13813–13821. [PubMed: 24160871]
13. Chen S, Goode AE, Sweeney S, Theodorou IG, Thorley AJ, Ruenraroengsak P, Chang Y, Gow A, Schwander S, Skepper J, Zhang JJ, Shaffer MS, Chung KF, Tetley TD, Ryan MP, Porter AE. Sulfidation of silver nanowires inside human alveolar epithelial cells: a potential detoxification mechanism. Nanoscale. 2013; 5:9839–47. [PubMed: 23970174]
14. Creuwels LA, van Golde LM, Haagsman HP. The pulmonary surfactant system: biochemical and clinical aspects. Lung. 1997; 175:1–39. [PubMed: 8959671]
15. Johansson J, Curstedt T, Robertson B. The proteins of the surfactant system. Eur Respir J. 1994; 7:372–91. [PubMed: 8162991]
16. Theodorou I, Ryan M, Tetley T, Porter A. Inhalation of Silver Nanomaterials—Seeing the Risks. International journal of molecular sciences. 2014; 15:23936–23974. [PubMed: 25535082]
17. Thorley AJ, Tetley TD. New perspectives in nanomedicine. Pharmacology & Therapeutics. 2013; 140:176–185. [PubMed: 23811125]
18. Geiser M, Schurch S, Gehr P. Influence of surface chemistry and topography of particles on their immersion into the lung's surface-lining layer. Journal of applied physiology. 2003; 94:1793–801. [PubMed: 12547838]
19. Mijailovich SM, Kojic M, Tsuda A. Particle-induced indentation of the alveolar epithelium caused by surface tension forces. 2010; 109:1179–1194.
20. Wells MA, Abid A, Kennedy IM, Barakat AI. Serum proteins prevent aggregation of Fe2O3 and ZnO nanoparticles. Nanotoxicology. 2012; 6:837–46. [PubMed: 22149273]
21. Harishchandra RK, Saleem M, Galla HJ. Nanoparticle interaction with model lung surfactant monolayers. Journal of the Royal Society, Interface / the Royal Society. 2010; 7(Suppl 1):S15–26.
22. Leo BF, Chen S, Kyo Y, Herpoldt KL, Terrill NJ, Dunlop IE, McPhail DS, Shaffer MS, Schwander S, Gow A, Zhang J, Chung KF, Tetley TD, Porter AE, Ryan MP. The stability of silver nanoparticles in a model of pulmonary surfactant. Environmental science & technology. 2013; 47:11232–40. [PubMed: 23988335]
23. Sun Y, Xia Y. Large-Scale Synthesis of Uniform Silver Nanowires Through a Soft, Self-Seeding, Polyol Process. Advanced Materials. 2002; 14:833–837.
24. Xia Y, Xiong Y, Lim B, Skrabalak SE. Shape-controlled synthesis of metal nanocrystals: simple chemistry meets complex physics? Angewandte Chemie. 2009; 48:60–103. [PubMed: 19053095]
25. Marambio-Jones C, Hoek EMV. A review of the antibacterial effects of silver nanomaterials and potential implications for human health and the environment. Journal of Nanoparticle Research. 2010; 12:1531–1551.
26. Eckhardt S, Brunetto PS, Gagnon J, Priebe M, Giese B, Fromm KM. Nanobio silver: its interactions with peptides and bacteria, and its uses in medicine. Chemical reviews. 2013; 113:4708–54. [PubMed: 23488929]
27. Cronholm P, Karlsson HL, Hedberg J, Lowe TA, Winnberg L, Elihn K, Wallinder IO, Moller L. Intracellular Uptake and Toxicity of Ag and CuO Nanoparticles: A Comparison Between Nanoparticles and their Corresponding Metal Ions. Small. 2013; 9:970–982. [PubMed: 23296910]
28. Li X, Lenhart JJ, Walker HW. Aggregation Kinetics and Dissolution of Coated Silver Nanoparticles. Langmuir : the ACS journal of surfaces and colloids. 2012; 28:1095–1104. [PubMed: 22149007]
29. Levard C, Hotze EM, Lowry GV, Brown GE Jr. Environmental Transformations of Silver Nanoparticles: Impact on Stability and Toxicity. Environmental science & technology. 2012; 46:6900–6914. [PubMed: 22339502]

30. Hayat MA. Principles and Techniques of Electron Microscopy Biological Applications (4th). 2000
31. Park S-H, Oh S-G, Mun J-Y, Han S-S. Effects of silver nanoparticles on the fluidity of bilayer in phospholipid liposome. Colloids and Surfaces B: Biointerfaces. 2005; 44:117–122. [PubMed: 16040237]
32. Leonenko ZV, Finot E, Ma H, Dahms TE, Cramb DT. Investigation of temperature-induced phase transitions in DOPC and DPPC phospholipid bilayers using temperature-controlled scanning force microscopy. Biophysical journal. 2004; 86:3783–93. [PubMed: 15189874]
33. Boonrungsiman S, Fearn S, Gentleman E, Spillane L, Carzaniga R, McComb DW, Stevens MM, Porter AE. Correlative spectroscopy of silicates in mineralised nodules formed from osteoblasts. Nanoscale. 2013; 5:7544–51. [PubMed: 23835574]
34. Liu JY, Hurt RH. Ion Release Kinetics and Particle Persistence in Aqueous Nano-Silver Colloids. Environmental science & technology. 2010; 44:2169–2175. [PubMed: 20175529]
35. Washio I, Xiong Y, Yin Y, Xia Y. Reduction by the End Groups of Poly(vinyl pyrrolidone): A New and Versatile Route to the Kinetically Controlled Synthesis of Ag Triangular Nanoplates. Advanced Materials. 2006; 18:1745–1749.
36. Kan C, Wang C, Zhu J, Li H. Formation of gold and silver nanostructures within polyvinylpyrollidone (PVP) gel. Journal of Solid State Chemistry. 2010; 183:858–865.
37. Glover, Richard D.; Hutchison, James E. Generation of Metal Nanoparticles from Silver and Copper Objects: Nanoparticle Dynamics on Surfaces and Potential Sources of Nanoparticles in the Environment. Acs Nano. 2011; 5:8950–8957. J. M. M., ‡. †,‡,*. [PubMed: 21985489]
38. Yu, S.-j.; Yin, Y.-g.; Chao, J.-b.; Shen, M.-h.; Liu, J.-f. Highly Dynamic PVP-Coated Silver Nanoparticles in Aquatic Environments: Chemical and Morphology Change Induced by Oxidation of Ag0 and Reduction of Ag+ Environmental science & technology. 2013; 48:403–411. [PubMed: 24328224]
39. Chappell MA, Miller LF, George AJ, Pettway BA, Price CL, Porter BE, Bednar AJ, Seiter JM, Kennedy AJ, Steevens JA. Simultaneous dispersion-dissolution behavior of concentrated silver nanoparticle suspensions in the presence of model organic solutes. Chemosphere. 2011; 84:1108–1116. [PubMed: 21550097]
40. MacCuspie RI, Allen AJ, Hackley VA. Dispersion stabilization of silver nanoparticles in synthetic lung fluid studied under in situ conditions. Nanotoxicology. 2011; 5:140–156. [PubMed: 21609136]
41. Stringer B, Kobzik L. Alveolar macrophage uptake of the environmental particulate titanium dioxide: role of surfactant components. American journal of respiratory cell and molecular biology. 1996; 14:155–60. [PubMed: 8630265]
42. Konduru NV, Tyurina YY, Feng W, Basova LV, Belikova NA, Bayir H, Clark K, Rubin M, Stolz D, Vallhov H, Scheynius A, Witasp E, Fadeel B, Kichambare PD, Star A, Kisin ER, Murray AR, Shvedova AA, Kagan VE. Phosphatidylserine Targets Single-Walled Carbon Nanotubes to Professional Phagocytes *In Vitro* and *In Vivo*. PLoS ONE. 2009; 4:e4398. [PubMed: 19198650]
43. Thorley AJ, Ruenraroengsak P, Potter TE, Tetley TD. Critical Determinants of Uptake and Translocation of Nanoparticles by the Human Pulmonary Alveolar Epithelium. Acs Nano. 2014; 8:11778–11789. [PubMed: 25360809]
44. Gasser M, Wick P, Clift MJ, Blank F, Diener L, Yan B, Gehr P, Krug HF, Rothen-Rutishauser B. Pulmonary surfactant coating of multi-walled carbon nanotubes (MWCNTs) influences their oxidative and pro-inflammatory potential in vitro. Particle and fibre toxicology. 2012; 9:17. [PubMed: 22624622]
45. Herzog E, Byrne HJ, Davoren M, Casey A, Duschl A, Oostingh GJ. Dispersion medium modulates oxidative stress response of human lung epithelial cells upon exposure to carbon nanomaterial samples. Toxicology and applied pharmacology. 2009; 236:276–281. [PubMed: 19233222]
46. Schulze C, Schaefer UF, Ruge CA, Wohlleben W, Lehr CM. Interaction of metal oxide nanoparticles with lung surfactant protein A. European journal of pharmaceutics and biopharmaceutics : official journal of Arbeitsgemeinschaft fur Pharmazeutische Verfahrenstechnik e.V. 2011; 77:376–83. [PubMed: 21056657]
47. Schleh C, Rothen-Rutishauser B, Kreyling WG. The influence of pulmonary surfactant on nanoparticulate drug delivery systems. European journal of pharmaceutics and biopharmaceutics :

official journal of Arbeitsgemeinschaft fur Pharmazeutische Verfahrenstechnik e.V. 2011; 77:350–2. [PubMed: 21195761]

48. Salvador-Morales C, Townsend P, Flahaut E, Vénien-Bryan C, Vlandas A, Green MLH, Sim RB. Binding of pulmonary surfactant proteins to carbon nanotubes; potential for damage to lung immune defense mechanisms. Carbon. 2007; 45:607–617.
49. Ruge CA, Schaefer UF, Herrmann J, Kirch J, Canadas O, Echaide M, Perez-Gil J, Casals C, Muller R, Lehr CM. The interplay of lung surfactant proteins and lipids assimilates the macrophage clearance of nanoparticles. PLoS One. 2012; 7:e40775. [PubMed: 22802970]
50. Suresh AK, Pelletier DA, Wang W, Morrell-Falvey JL, Gu B, Doktycz MJ. Cytotoxicity Induced by Engineered Silver Nanocrystallites Is Dependent on Surface Coatings and Cell Types. Langmuir : the ACS journal of surfaces and colloids. 2012; 28:2727–2735. [PubMed: 22216981]
51. Oh W-K, Kim S, Choi M, Kim C, Jeong YS, Cho B-R, Hahn J-S, Jang J. Cellular Uptake, Cytotoxicity, and Innate Immune Response of Silica−Titania Hollow Nanoparticles Based on Size and Surface Functionality. Acs Nano. 2010; 4:5301–5313. [PubMed: 20698555]
52. Wang X, Ji Z, Chang CH, Zhang H, Wang M, Liao Y-P, Lin S, Meng H, Li R, Sun B, Winkle LV, Pinkerton KE, Zink JI, Xia T, Nel AE. Use of Coated Silver Nanoparticles to Understand the Relationship of Particle Dissolution and Bioavailability to Cell and Lung Toxicological Potential. Small. 2014; 10:385–398. [PubMed: 24039004]
53. Carlson C, Hussain SM, Schrand AM, Braydich-Stolle LK, Hess KL, Jones RL, Schlager JJ. Unique Cellular Interaction of Silver Nanoparticles: Size-Dependent Generation of Reactive Oxygen Species. The Journal of Physical Chemistry B. 2008; 112:13608–13619. [PubMed: 18831567]
54. Zhang W, Yao Y, Sullivan N, Chen Y. Modeling the Primary Size Effects of Citrate-Coated Silver Nanoparticles on Their Ion Release Kinetics. Environmental science & technology. 2011; 45:4422–4428. [PubMed: 21513312]

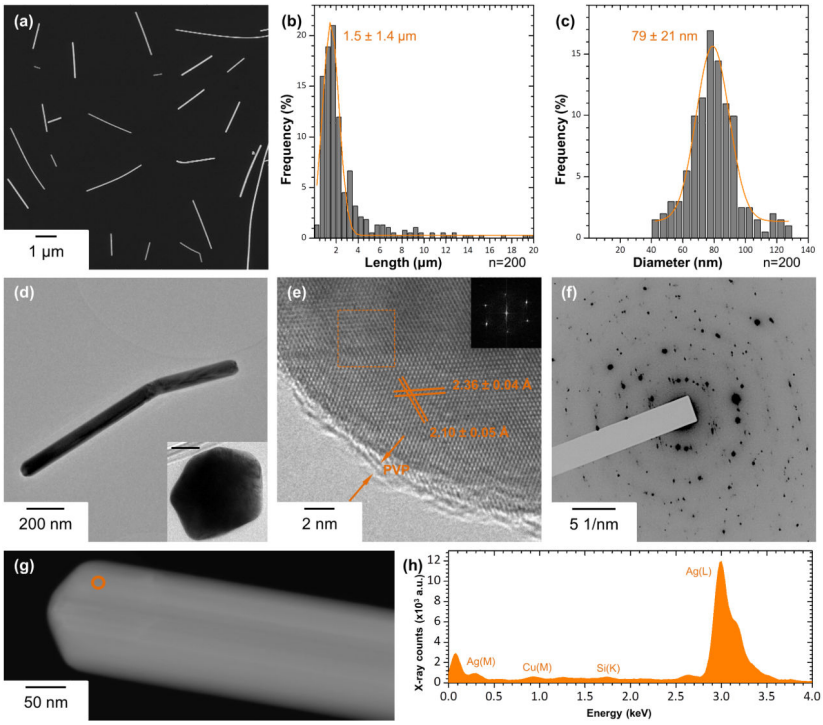

Figure 1.

Physicochemical characterization of the as-synthesized AgNWs by SEM, TEM, SAED and STEM/EDX. (a) SEM image of as-synthesized AgNWs, and their length (b) and diameter (c) distributions. The curves represent the Gaussian fit to the data. (d) A low-resolution BFTEM image of AgNWs. Inset shows the cross section of AgNWs, scale bar 30 nm. (e) High-resolution BFTEM image of a single AgNW, showing its crystal structure and the PVP capping on its surface. Inset is the corresponding FFT pattern taken from the boxed area (f) SAED pattern taken from an area containing multiple AgNWs. (g) HAADF-STEM image of a single AgNW and (h) the corresponding STEM/EDX spectrum collected from the area circled in (g).

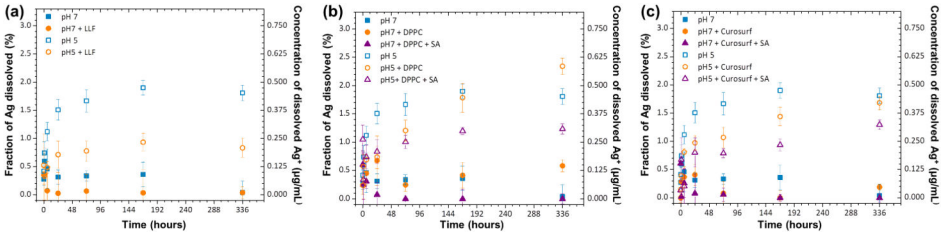

Figure 2.

(a-c) ICP-OES analysis of the amount of free Ag^{+} ions released from AgNWs in complete LLF (a) and individual LLF components (b, c). AgNWs were incubated in perchlorate buffer solutions (pH7 and pH5), in the presence and absence of LLF (a), DPPC ± SA (b) or Curosurf® ± SA (c), for 1 hour up to 336 hours (14 days).

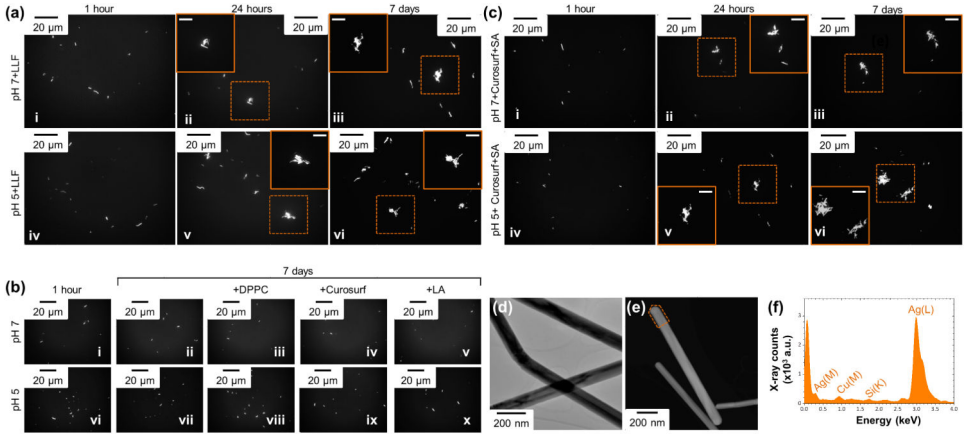

Figure 3.

(a) Reflectance mode optical images of AgNWs incubated with LLF at pH 7 (i-iii) and pH 5 (iv-vi), for 1 hour (i, iv), 24 hours (ii, v) and 7 days (iii, vi). (b) Reflectance mode optical images of AgNWs incubated at pH 7 (i-v) and pH 5 buffers (vi-x), in the absence (i, ii, vi and vii) and presence of DPPC (iii and viii), Curosurf® (iv and ix) and LA (v and x). (b) Reflectance mode optical images of AgNWs incubated with Curosurf® and SA at pH 7 (i-iii) and pH 5 (iv-vi), for 1 hour (i, iv), 24 hours (ii, v) and 7 days (iii, vi). (c) A BFTEM image of AgNWs incubated at pH 5 for 14 days. (d) A STEM image and (e) a STEM/EDX spectrum from the area marked in (d) of AgNWs incubated with SA for 24 hours.

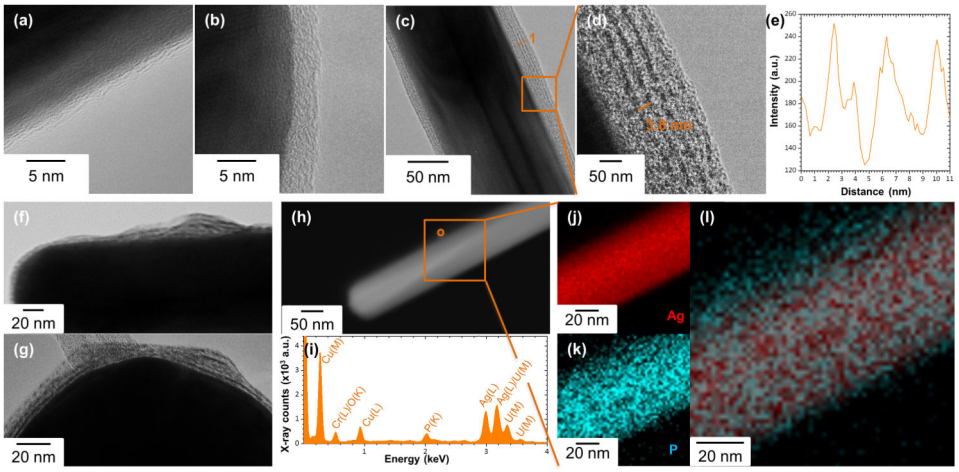

Figure 4.

(a-d and f-g) BFTEM images of AgNWs incubated in pH7 buffer (a), with DPPC (b-d), Curosurf® (f) and LA (g). In (c, d) and (f-h) samples were positively stained with uranyl acetate to enhance phospholipid contrast. (d) Magnification of the area boxed in (c), showing the phospholipid bilayers formed on the surface of AgNWs. (e) Intensity line profile collected from the line marked 1 in (c). (h) HAADF-STEM image of a single AgNW and (i) corresponding EDX spectrum collected from the area circled in (h), confirming the presence of phosphorus on the surface of AgNWs. (j-l) The boxed area in (h) was further characterized by STEM/EDX (j) silver (Ag) and (k) phosphorus (P) elemental mapping. (l) The overlaid image confirms that AgNWs are wrapped by phospholipids.

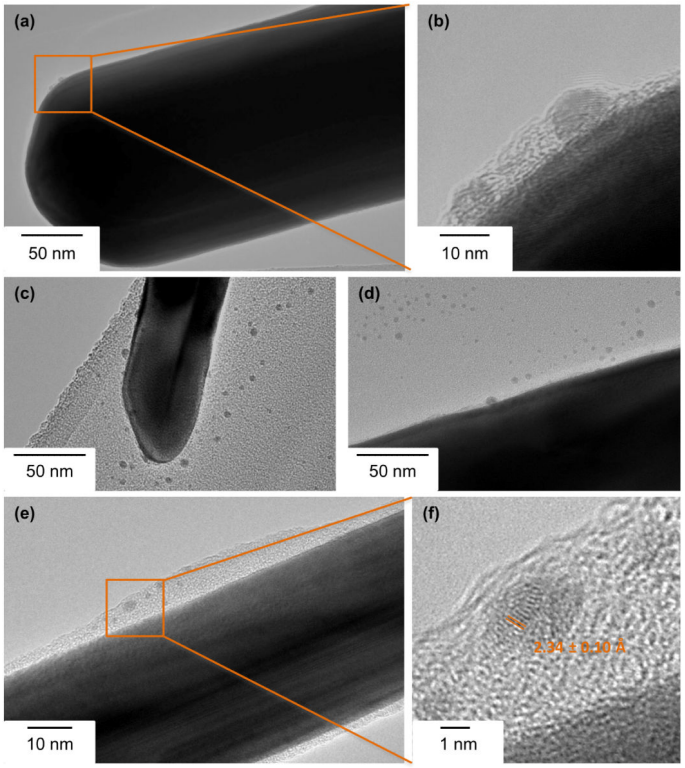

Figure 5.

BFTEM images of AgNWs showing the generation of a secondary population of nanoparticles. (a) Small nanoparticles were formed at the surface of AgNWs after incubation in pH 7 perchlorate buffers for 24 hours. (b) The magnification of the boxed area in (a) shows that the particles formed are trapped in the PVP capping layer of AgNWs. (c) AgNWs incubated at pH 7 for 1 week. A larger amount of nanoparticles was observed, close to the surface of AgNWs and in several areas of the carbon coating of the TEM grid. (d) AgNWs incubated at pH5 for 7 days. (e) AgNWs incubated at pH7 in the presence of DPPC for 24 hours. The amorphous layer around the AgNWs corresponds to the phospholipid wrapping of the wires. (f) The magnification of the boxed area in (e) shows that crystalline nanoparticles are present inside the phospholipid coating.

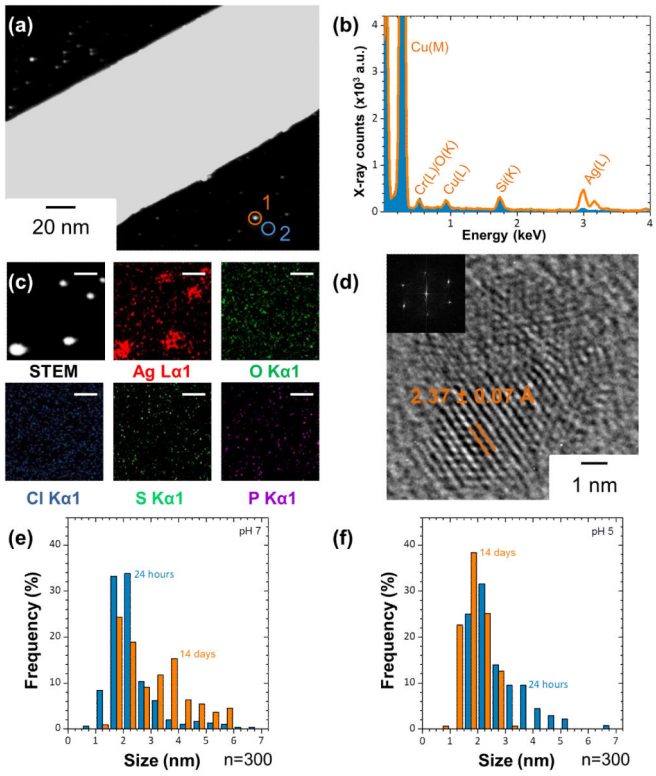

Figure 6.

HAADF STEM imaging, STEM/EDX elemental analysis and mapping and HRTEM characterization of the secondary nanoparticles from the original AgNWs. (a) STEM image of AgNWs incubated in pH7 perchlorate buffers for 7 days. The image reveals the presence of a large number of small particles on the surface and around the AgNWs. (b) STEM/EDX spectrum of a single nanoparticle, collected from the circled area 1 in (a) and comparison with the background spectrum, collected from the circled area 2 in (a). (c) HAADF STEM imaging and EDX elemental mapping. Scale bar 10 nm. (d) HRTEM of nanoparticles formed after the incubation of AgNWs at pH7 for 7 days. The lattice spacing of the nanoparticles corresponds to that of metallic Ag (111). (e-f) Size distribution of the AgNPs generated after the incubation of AgNWs at pH7 (e) and pH5 (f), for 24 hours and 14 days.